Restoration of Aqua MODIS Band 6 Using Histogram Matching and Local Least Squares Fitting

Preesan Rakwatin, Wataru Takeuchi, and Yoshifumi Yasuoka, *Senior Member, IEEE*

***Abstract*—The MODerate resolution Imaging Spectrometer (MODIS) aboard Terra and Aqua platforms is performing well overall, except for Aqua MODIS band 6. Fifteen of the 20 detectors in Aqua MODIS band 6 are nonfunctional or noisy. Without correction, it will cause problems in the higher MODIS products. This paper develops a restoration algorithm to restore the missing data of Aqua MODIS band 6 by combining a histogram-matching algorithm with local least squares fitting. Histogram matching corrects detector-to-detector striping of the functional detectors. Local least squares fitting restores the missing data of the nonfunctional detector based on a cubic polynomial derived from the relationship between Aqua MODIS bands 6 and 7. The Aqua MODIS image data used in this research are in digital number format and are not georectified. The proposed restoring algorithm can be used on both 1000- and 500-m pixel resolutions. The algorithm was tested on both Terra and Aqua MODIS images. For Terra MODIS images, results of restoring the synthetic nonfunctional detectors of band 6 demonstrate that local least squares fitting can fill in the missing data with little distortion. For Aqua MODIS images, the results of the restoring algorithm with and without applying histogram matching were compared to evaluate the capability in removing detector-to-detector stripe noise. To evaluate the performance of the proposed method, quantitative and qualitative analyses were carried out by visual inspection and quality index. For all the scenes used in this research, the correlation coefficients were near 0.99 and root mean square error between the original Terra band 6 and its simulated one was 2×10^{-5}. The proposed algorithm can thus be used satisfactorily for restoring Aqua MODIS band 6.**

***Index Terms*—Aqua, band 6, histogram matching, local least squares fitting, MODerate resolution Imaging Spectrometer (MODIS).**

I. Introduction

THE MODERATE resolution Imaging Spectroradiometer (MODIS) is the main instrument aboard the Earth Observing System (EOS) mission. It has been designed to provide data for global monitoring of land, ocean, and atmosphere [1], [3], [6], [9]. MODIS aboard the Terra spacecraft has been operated since its launch in December 1999; the MODIS aboard the EOS Aqua spacecraft has been in operation since May 2002. The Terra spacecraft orbits the globe and passes from north to south (descending) across the equator at 10:30 A.M., while the Aqua spacecraft passes south to north (ascending) over the equator at 1:30 P.M. MODIS observes the Earth using 36 spectral bands covering wavelengths from visible (VIS) to long-wave infrared. It has three different nadir ground spatial resolutions: 250 (bands 1 and 2), 500 (bands 3 to 7), and 1000 m (bands 8 to 36). MODIS is a cross-track scanning radiometer using a double-sided scanning mirror to view onboard calibrators and the Earth. The 250-m spatial resolution band uses 40 detectors; the 500-m spatial resolution band, 20 detectors; and the 1000-m spatial resolution band, 10 detectors.

The prelaunch developed characteristics and algorithms of Terra MODIS that were described in [1] and [2] provide more specific information about Terra and Aqua MODIS. The orbit characteristics of Terra MODIS are presented in [4]–[11]. The current performance and status of both Terra and Aqua MODIS can be checked on the MODIS homepage (http://modis.gsfc.nasa.gov) and the MODIS Characterization Support Team homepage (http://www.ncst.ssai.biz) [7].

The Aqua MODIS instrument has performed well except for band 6 (1.628–1.652 μm). Specifically, 15 of the 20 detectors in Aqua MODIS band 6 are nonfunctional or noisy [13], [14]. Furthermore, the remaining functional detectors are contaminated by detector-to-detector striping. Detector-to-detector striping can be detected as a pattern of sharp repetitive stripes over an entire image [18]. The detector-to-detector striping is mainly caused by relative gain and/or offset differences among detectors within a band [17], [18], [20], [21]. Another cause is that photomultipliers are nonlinear and their response depends on their exposure history [24].

MODIS band 6 is an important band used in the following MODIS products and applications. Over the ocean, two aerosol products are derived from MODIS using different sampling and aerosol algorithms. The primary or M product is derived from the standard multispectral aerosol product developed by the MODIS aerosol group. A simpler secondary [AVHRR-like] or A product is derived by the CERES Science Team using a different cloud-clearing method and a single-channel aerosol algorithm. Two aerosol optical depths τ_{A1} and τ_{A2} are derived from MODIS bands 1 (0.62–0.67 μm) and 6. On Aqua, the retrievals are made in band 7 (2.105–2.155 μm) because of poor quality data from band 6 [27]–[29].

For the snow-mapping and cloud-mask algorithms, MODIS band 6 is used to calculate the normalized difference snow index (NDSI) [30]–[34]. NDSI is formulated as the difference of reflectance in the VIS band such as MODIS band 4 (0.545–0.565 μm) and short-wave infrared (SWIR) band such

Manuscript received March 5, 2008; revised June 29, 2008. First published December 2, 2008; current version published January 28, 2009. This work was supported by the Japan Science and Technology under the Research Project Solution Oriented Research for Science and Technology.

P. Rakwatin is with the Earth Observation Research Center, Space Applications Mission Directorate, Japan Aerospace Exploration Agency, Tsukuba 305-8505, Japan (e-mail: rakwatin.preesan@jaxa.jp).

W. Takeuchi is with the Institute of Industrial Science, The University of Tokyo, Tokyo 153-8505, Japan (e-mail: wataru@iis.u-tokyo.ac.jp).

Y. Yasuoka is with the National Institute for Environmental Studies, Tsukuba 305-8506, Japan (e-mail: yasuoka@nies.go.jp).

Color versions of one or more of the figures in this paper are available online at http://ieeexplore.ieee.org.

Digital Object Identifier 10.1109/TGRS.2008.2003436

as MODIS band 6 divided by the sum of those reflectances. On Aqua MODIS, band 7 has been used to calculate NDSI instead of band 6, since snow has similar reflectance characteristics in MODIS bands 6 and 7 relative to other bands [32].

Salomonson and Appel [13] developed and validated an algorithm to estimate the fractional snow cover (FRA) using 500-m-per-pixel-resolution data from Aqua MODIS instruments. The FRA7 relationship employed the NDSI calculated from Aqua MODIS band 7 instead of band 6. The FRA7 relationship had to be developed because the quality of band 6 data on the Aqua MODIS instrument is poor due to the majority of the detectors being nonfunctional. The resulting equation is

$$\text{FRA7} = -0.64 + 1.91 * \text{NDSI7} \tag{1}$$

where FRA7 is the fractional snow cover and NDSI7 is the normalized difference snow index using MODIS band 7 in place of band 6.

The 1.65-μm spectrum region absorbed by ice particles [35] is detected to determine cloud overlap. Thus, the reflectance at 1.65 μm received by the detector is much stronger than water particles. This means that optically thick water clouds are brighter than the optically thick ice clouds observed in the MODIS band 6 images. For this reason, MODIS band 6 is used with some specified thresholds to detect high-ice-content clouds and lower water-content clouds [35]–[39].

MODIS band 6 has proven to be particularly important for forest biomass estimation and canopy water stress. Previous studies identified the utility of SWIR data for estimating forest canopy structure variables [41]–[44]. Baccini *et al.* [41] mentioned a strong negative relationship between biomass and MODIS band 6 reflectance. Fenholt and Sandholt [40] derived an SWIR water stress index using MODIS band 6 as one of its inputs. This is because leaf water is strongly absorbed at the SWIR wavelengths and the reflectance from plants is thus negatively related to leaf water content.

As discussed in the previous paragraphs, Aqua MODIS band 6 must be restored for MODIS products and for consistency in observing the Earth. The principal purpose of this research is to develop and evaluate a method for restoring Aqua MODIS band 6 using histogram matching and local least squares fitting. Histogram matching is used for detector-to-detector destriping of the functional detectors. Local least squares fitting is used for retrieving the missing data of the nonfunctional detectors. The Aqua MODIS image data used in this research are in digital format and are not georectified. The proposed method can be applied for both 1000- and 500-m pixel resolutions. The Aqua band 6 retrieving results are validated quantitatively and qualitatively to demonstrate the performance of the proposed restoration algorithm.

This paper is organized as follows. Section II describes the past efforts to develop an Aqua MODIS band 6 restoration method. Section III introduces a proposed Aqua MODIS band 6 restoration procedure using histogram matching and local least squares fitting. The experimental results and validation of both Terra MODIS and Aqua MODIS images are subsequently presented in Section IV. Finally, Section V gives a summary and conclusion of this research.

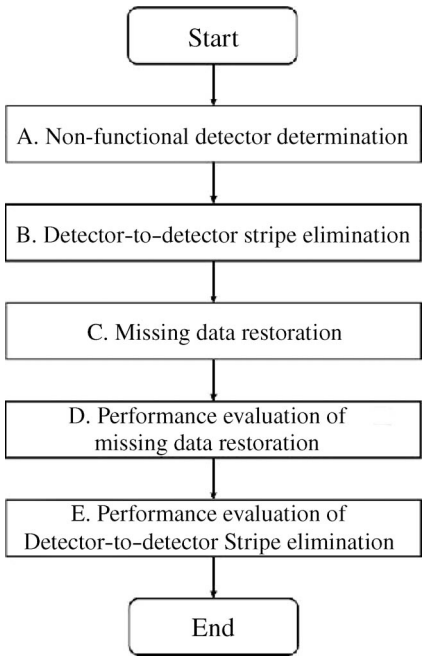

Fig. 1. Flow diagrams of the procedure to restore Aqua MODIS band 6.

II. Previous Aqua MODIS Band 6 Restoration Algorithm

Until now, only one article has been available on the Aqua MODIS band 6 retrieving algorithm. Wang *et al.* [14] demonstrated an approach for restoring Aqua MODIS band 6 using the analytical relationship between Terra MODIS bands 6 and 7. This is based on MODIS bands 6 and 7 being highly correlated and the relationship being stable over snow coverage. The algorithms for restoring Aqua MODIS band 6 were developed using Terra MODIS Level 1B calibrated and geolocated radiance. Polynomial regression was used to quantify the relationship between MODIS bands 6 and 7. Reflectances at the top of the atmosphere (TOA) in Terra MODIS bands 6 and 7 were correlated with correlation coefficients of 0.9821, and those of NDSI using band 6 and 7 were correlated with a correlation coefficient of 0.9777. Linear, quadratic, cubic, and fourth-degree polynomials were fit to the data of Terra bands 6 and 7. Wang *et al.* [14] suggested using the following cubic polynomials

$$\mathbf{R}_{B6} = 1.6032\mathbf{R}_{B7}^3 - 1.9458\mathbf{R}_{B7}^2 + 1.7948\mathbf{R}_{B7} + 0.012396. \tag{2}$$

Here, $\mathbf{R}_{B6}$ is the reflectance at TOA in Terra MODIS band 6, and $\mathbf{R}_{B7}$ is that in band 7.

However, the relationship between these two bands also depends on many factors, such as land cover types, spectral characteristics, and scan geometry. Wang *et al.* [15] found that land cover types play an important role in the relationship between MODIS bands 6 and 7. The aforementioned equation was developed based on snow cover; therefore, its performance benefits cases with snow cover, but has relatively large errors in cases without snow cover. The accuracy of snow mapping is related to how well the retrieving algorithm can represent the original band 6. In addition, the setting of the NDSI threshold for snow mapping is very important. Wang *et al.* [15] took

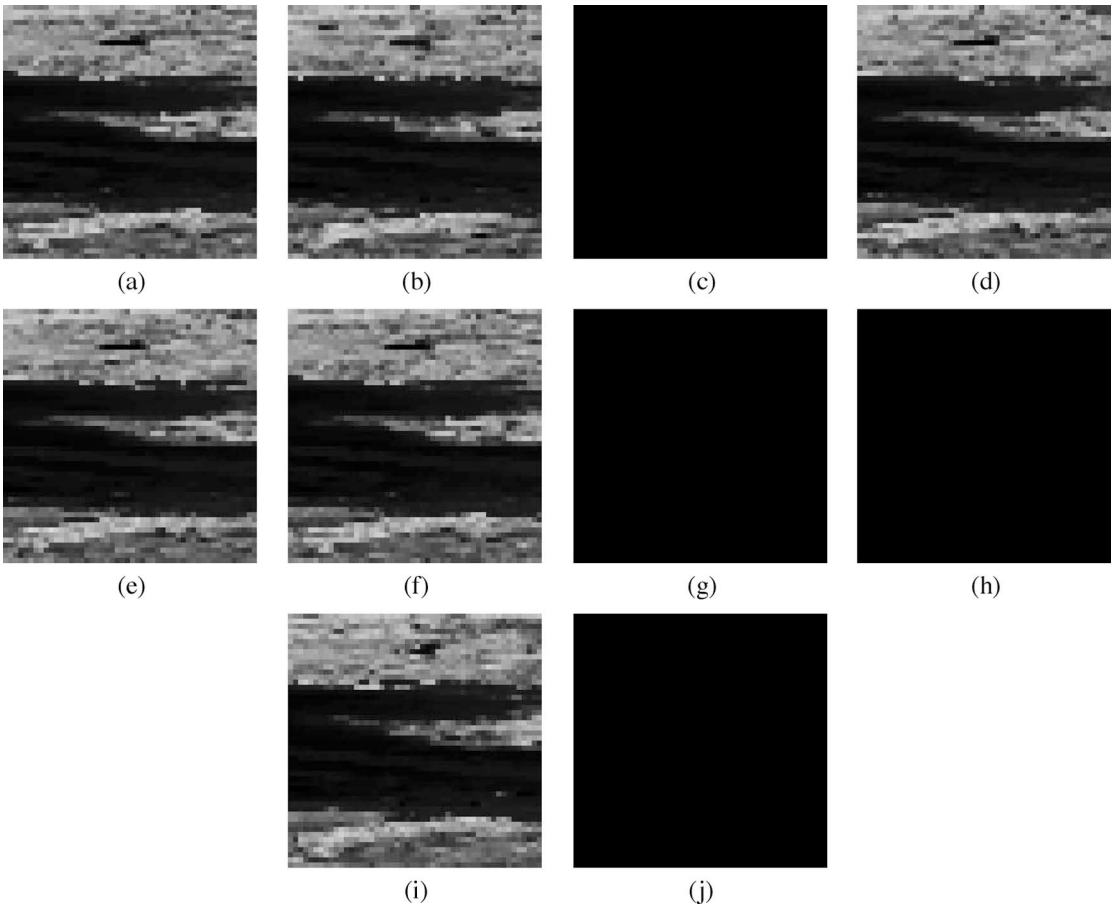

Fig. 2. Ten detector subimages derived from the Aqua MODIS band 6 image acquired on June 11, 2005. Each detector subimage has 200 by 200 pixels. (a)–(j) First to tenth detector subimages, respectively.

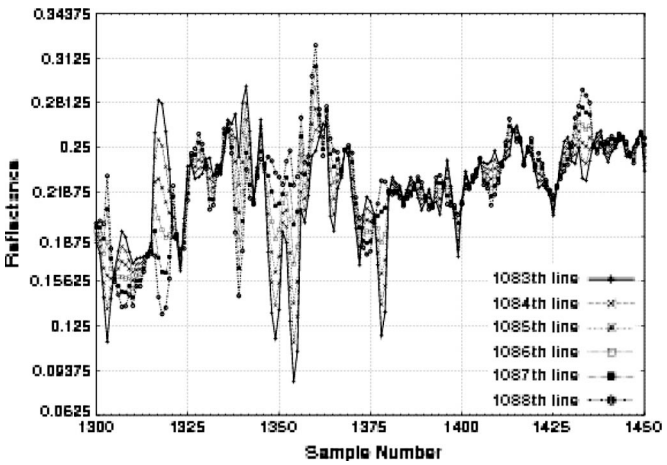

Fig. 3. Sample plot of the along-track column data extracted from Aqua MODIS band 6 at 500-m pixel resolution. Image was acquired on June 11, 2005. The 1084th–1087th lines were interpolated from the 1083rd and 1088th lines.

0.4 (0.54) as the threshold of NDSI for band 6 (band 7). However, these values may vary in different situations [15].

III. Data Processing

In this research, Terra and Aqua MODIS data were obtained from the Institute of Industrial Science (IIS), The University of

1	71	16	67	11	92	87
60	10	91	78	11	6	54
89	21	45	8	98	70	34
64	63	90	38	36	56	25
28	60	3	59	10	42	19
54	92	49	69	27	80	36

Band 6

5	145	35	137	25	187	177
123	23	185	159	25	15	111
181	45	93	19	199	143	71
131	47	29	15	117	179	187
131	129	183	79	75	115	53
59	123	9	121	23	87	41
111	187	101	141	57	163	75

Band 7

Fig. 4. Example of rectangular region between Aqua MODIS bands 6 and 7.

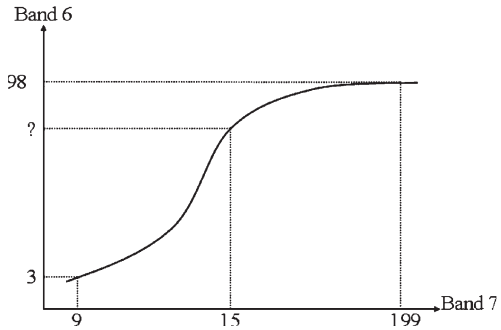

Fig. 5. Example of local cubic polynomial graph between Aqua MODIS bands 6 and 7.

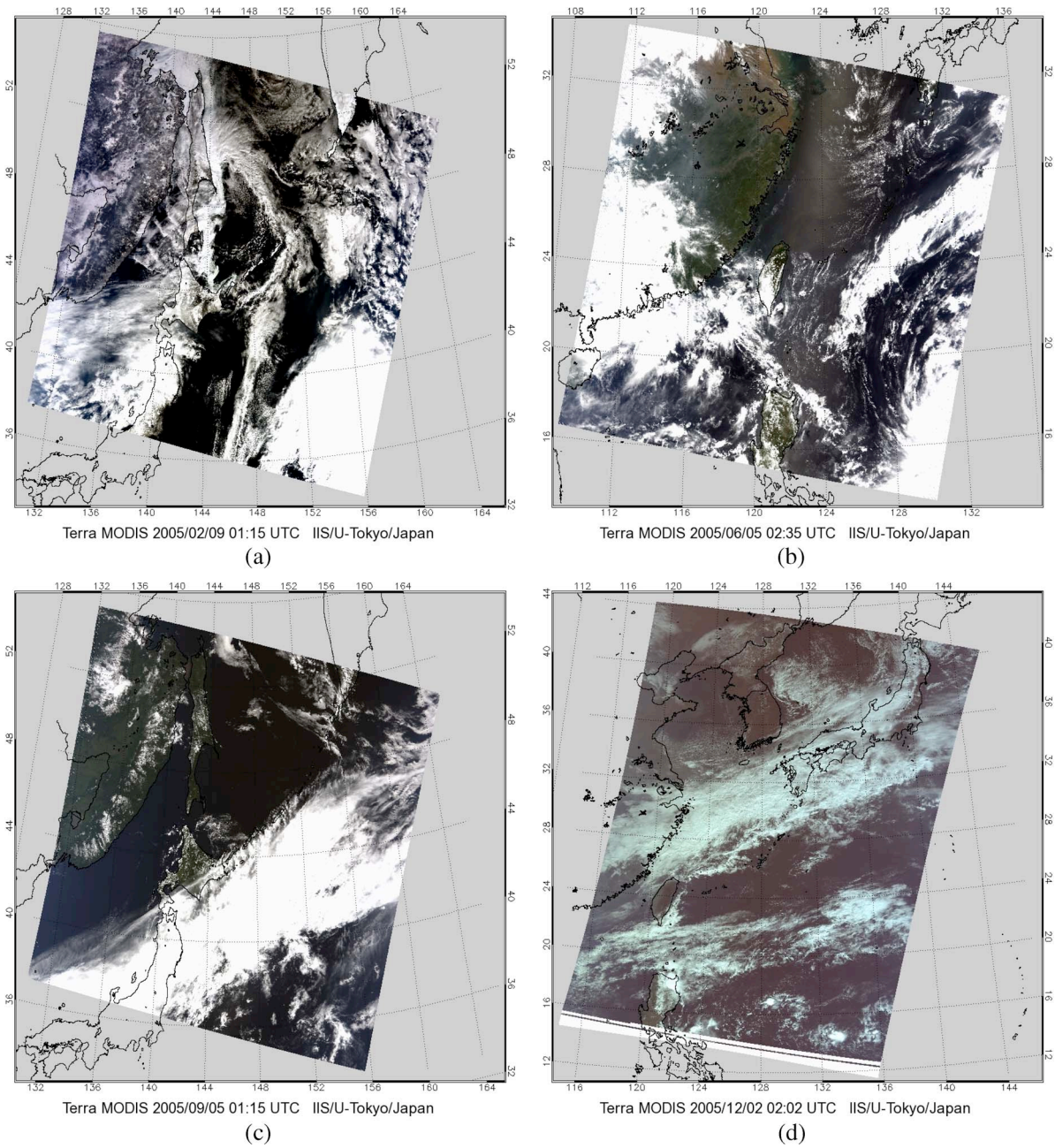

Fig. 6. Terra MODIS images showing areas that were used to test the proposed algorithm. Images were acquired on (a) February 9, 2005, (b) June 5, 2005, (c) September 5, 2005, and (d) December 2, 2005.

Tokyo, on the direct broadcasting system. The original level 0 data are converted to level 1B data by SeaWiFS Data Analysis System software (SEADAS, version 4). Level 1B data are in hierarchical data format (HDF)-EOS, which is the standard data format of Terra and Aqua MODIS sensors. MODIS data are in the form of 12-b precision brightness counts and coded to a 16-b scale. MODIS images are freely available on the URL http://webmodis.iis.u-tokyo.ac.jp/.

The procedure for restoring Aqua MODIS band 6 consists of three steps: 1) determine the nonfunctional detector; 2) eliminate the detector-to-detector stripe; and 3) restore missing data of Aqua MODIS band 6. The processing steps in the proposed algorithm are shown in the flow diagram in Fig. 1. The proposed algorithm for restoring Aqua MODIS band 6 can be used on both 500- and 1000-m-pixel-resolution data. The data are in 16-b integer values and must maintain scanning geometry.

A. *Nonfunctional Detector Determination*

To determine the nonfunctional pixels of a 1000-m-pixel-resolution image, we assume that the 1000-m-pixel-resolution image is created from ten detectors in the along-track direction and the first row of the original image is produced by the first detector of the MODIS sensor [20]. MODIS data are separated into ten subimages by the ten rows of scan detectors. However, each MODIS band 6's pixel at 1000-m resolution is actually formed via aggregation of four 500-m-pixel resolutions and

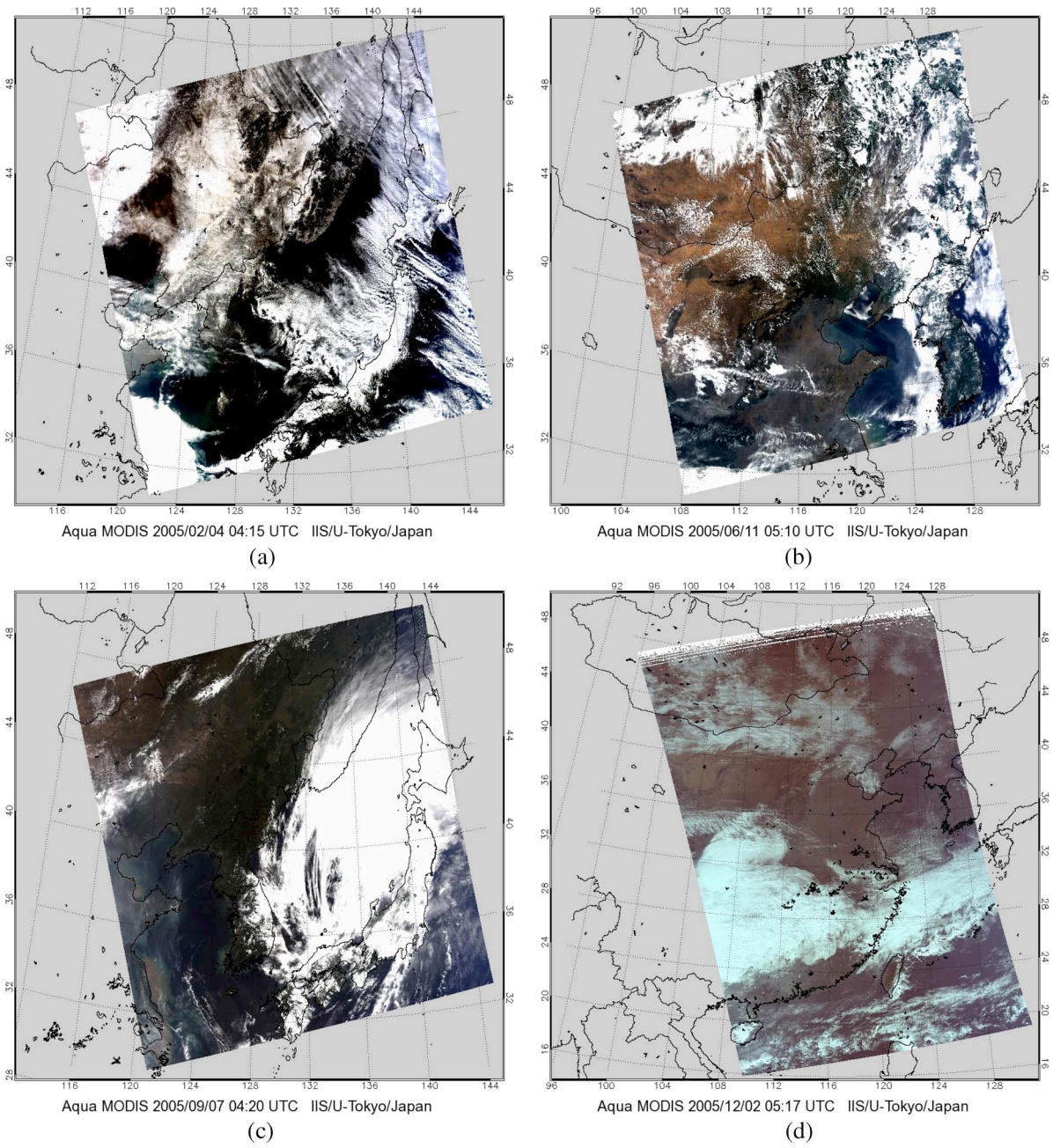

Fig. 7. Aqua MODIS images showing areas that were used to test the proposed algorithm. Images were acquired on (a) February 2, 2005, (b) June 11, 2005, (c) September 7, 2005, and (d) December 2, 2005.

therefore uses two of the 500-m detectors sampled twice each. Fig. 2 shows the ten subimages of the Aqua MODIS band 6 image acquired on June 11, 2005. Each subimage covers 200 by 200 pixels. The nonfunctional line pixels were identified by a visual interpretation. Fig. 2 shows that the previously shown image has nonfunctional pixels in the third, seventh, eighth, and tenth subimages. The nonfunctional subimages are dark and have a digital number (DN) of 65531.

To determine the missing data of the 500-m-pixel-resolution image, we should not use the same method as employed for the 1000-m-pixel-resolution image because a valid scaled integer value of a missing pixel was interpolated from the nearest functional detectors within the same scan [12]. The information of nonfunctional and noisy detectors is available in the global attributes of the HDF-EOS metadata. The attribute names are "Dead Detector List" and "Noisy Detector List," which list detectors that do not provide data of useful quality. There is a number of 490 detectors indexed by MODIS band and detector (1 = dead/noisy or 0 = not dead/not noisy) [12]. Fig. 3 shows the pixels along the line of Aqua MODIS band 6 at 500-m pixel resolution acquired on June 11, 2005. The 1083rd to 1088th lines were derived from the third to the eighth detectors. From HDF-EOS metadata, the third and eighth detectors are functional detectors but the rest are not. The 1084th to 1087th lines were created by the interpolating lines 1083 and 1088, respectively. The variation and amplitude of the fourth to the seventh detectors depend on the variation and amplitude of both the third and eighth detectors. For this reason, the

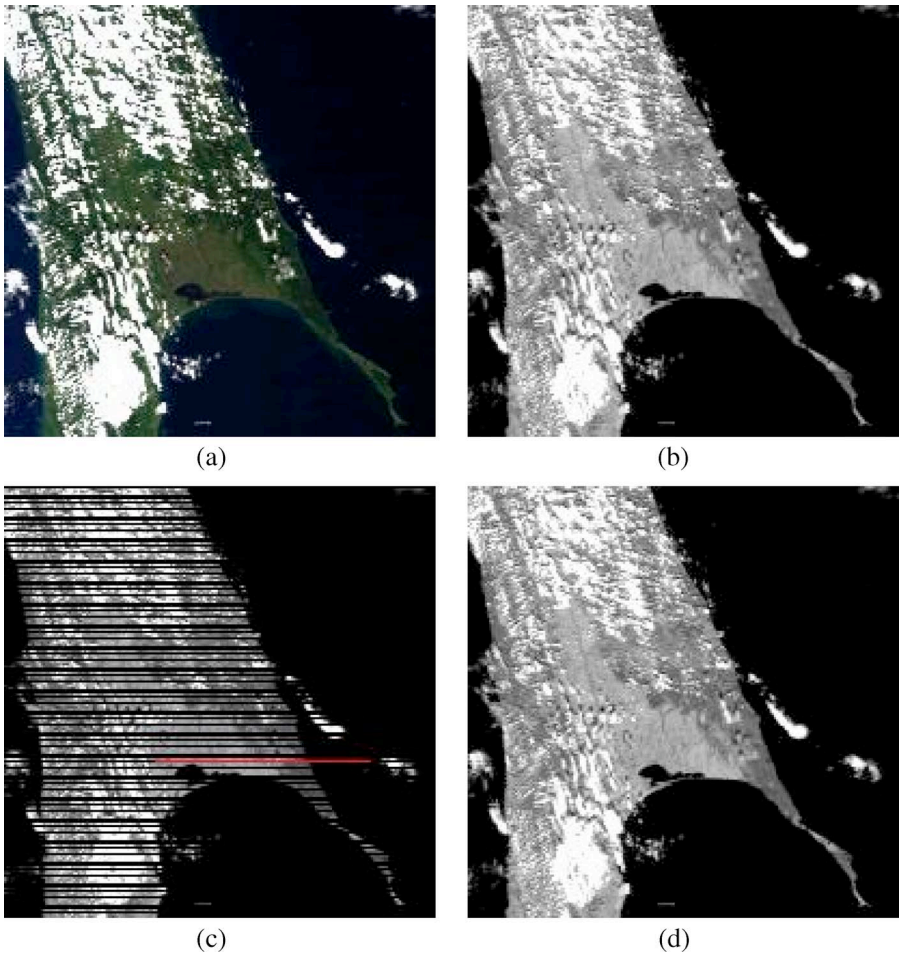

Fig. 8. Subimages of Terra MODIS of 1000-m pixel resolution acquired on September 5, 2005, over Sakhalin Island, Russia. These images are 200 by 200 pixels (200 by 200 km). (a) True color composite $R =$ band1, $G =$ band4, $B =$ band3, (b) original Terra MODIS band 6, (c) synthetic nonfunctional detector image, and (d) restored Terra MODIS band 6.

amplitude of the 1084th to 1087th lines in Fig. 3 varies in proportion to the variation of the 1083rd and 1088th lines.

B. Detector-to-Detector Stripe Elimination

To eliminate a detector-to-detector striping, Aqua MODIS data are processed using ten along-track (aggregate) pixels for 1000-m-resolution data and 20 along-track (detector) pixels for 500-m-resolution data. A cumulative distribution function (CDF) of each detector is prepared to match the CDF of a reference detector (a functional detector). A histogram-matching algorithm is based on the assumption that the distribution of the intensity of Earth radiation incident on each detector is similar over a large scene [21].

A histogram matching maps a CDF of each detector to a reference CDF. A normalization lookup table is created for each detector to map every DN x to a referenced DN x'. If $p_i(x)$ is the histogram of the output of the ith detector, the CDF of the ith detector $P_i(x)$ is

$$P_i(x) = \sum_{t=0}^{x} p_i(t). \tag{3}$$

CDF is a nondecreasing function of x, and its maximum value is unity. The basic assumption is that the CDF of each detector is a monotonic function. For each output value x of the ith detector, the value x' should satisfy

$$P_r(x') = P_i(x) \tag{4}$$

where subscript r refers to the reference detector. Therefore, a modified DN x' can be obtained from

$$x' = P_r^{-1}\left(P_i(x)\right). \tag{5}$$

Histogram matching has successfully been applied to satellite data such as Landsat Multispectral Scanner [21], Landsat Thematic Mapper [22], MODIS [16], [20], and Geostationary Operational Environmental Satellites [23].

C. Missing Data Restoration

The algorithm for restoring missing data on Aqua MODIS band 6 for both 500- and 1000-m pixel resolutions uses a gray-level transformation at each pixel of the nonfunctional detectors in the Aqua MODIS band 6 images. A polynomial regression was used to quantify the relationship between Aqua MODIS bands 6 and 7. The grayscale transformation is calculated by cubic polynomial determined from a least squares polynomial fitting. This research uses the "*POLY_FIT*" function package

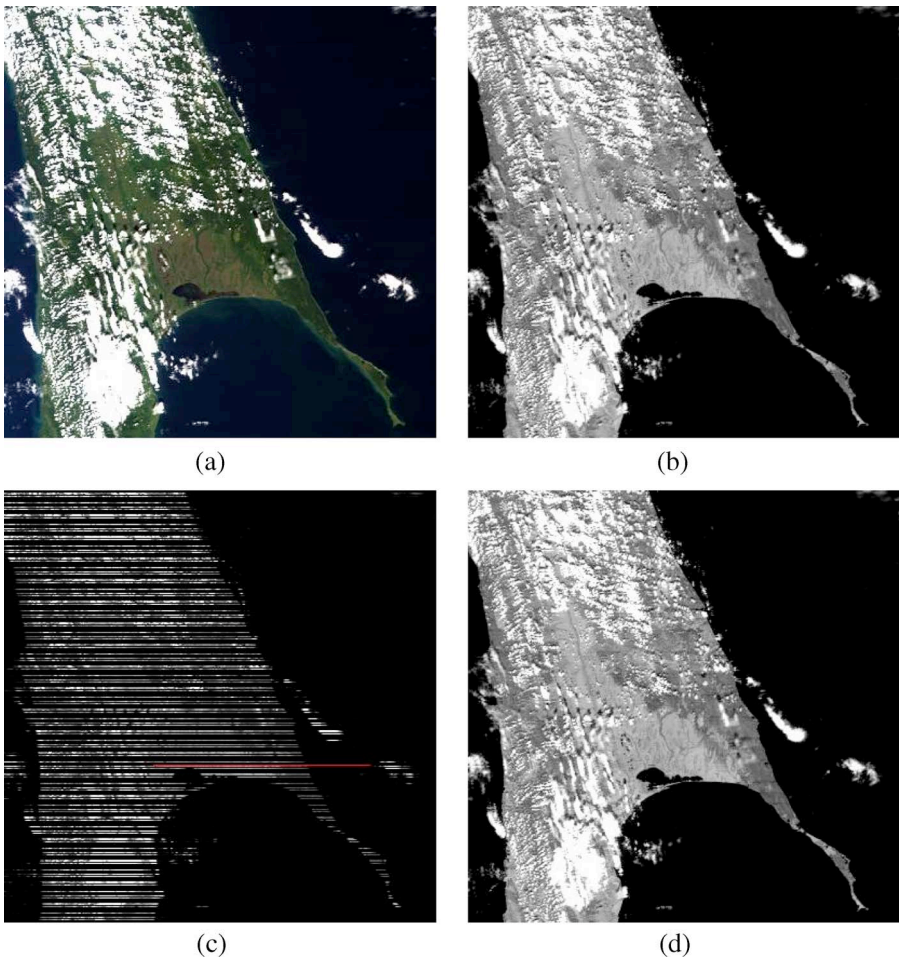

Fig. 9. Same as Fig. 8 except for 500-m pixel resolution, and this image is 400 by 400 pixels (200 by 200 km).

implemented in Interactive Data Language (IDL) to derive the cubic polynomial. The *POLY_FIT* routine uses matrix inversion to determine the coefficient. Even though IDL mentions that there are different versions of fitting routines that are more flexible and robust, the result of the *POLY_FIT* function routine is quite satisfactory for this application, and its computational time is much less than that of the others.

The steps involved in the restoring algorithm are as follows.

1) For each nonfunctional center pixel, determine the maximum and minimum values of the Aqua MODIS band 7 pixels from a defined rectangular region corresponding to the functional pixels of Aqua MODIS band 6. The initial rectangular region is set to a 15 $\times$ 3 window, 15 pixels long, and 3 pixels wide.
2) If the center pixel of Aqua MODIS band 7 in the rectangular region is neither larger nor smaller than the maximum and minimum values, then the local cubic polynomial function of the defined rectangular region is calculated from the pixel for which both bands 6 and 7 are still functional. If not, enlarge the rectangular region until the criteria are met.
3) Slide the rectangular window to the next nonfunctional pixel and repeat the aforementioned procedure.

For example, Fig. 4 shows the defined rectangular region of Aqua MODIS bands 6 and 7 that corresponded with each other. For band 7, the central pixel (shown in red) in the initial 5 $\times$ 3 rectangular region (shown in yellow) is lower than the minimum value of the surrounding pixel (value is 19). The rectangular window is enlarged to 7 $\times$ 5 where the center pixel is between the maximum value, 199, and minimum value, 9. The cubic polynomial function is then calculated from the IDL *POLY_FIT* function shown in Fig. 5. Finally, the center pixel of Aqua MODIS band 6 is replaced by the value calculated from the polynomial function.

IV. Results and Discussion

Four granule MODIS data of both Terra and Aqua were selected from different quarters to test the performance of the algorithms. For Terra MODIS, the selected data were acquired on February 9, June 5, September 5, and December 2, 2005. For Aqua MODIS, the data were taken on February 4, June 11, September 7, and December 2, 2005. This study used the data received at the IIS receiving station covering from the Pacific Ocean to Inner Mongolia. Terra (Aqua MODIS) image test scenes of this research are shown in Fig. 6 (Fig. 7).

A. Performance Evaluation of Missing Data Restoration

Synthetic Aqua MODIS band 6 images using Terra MODIS band 6 have been generated for both 1000- and 500-m pixel

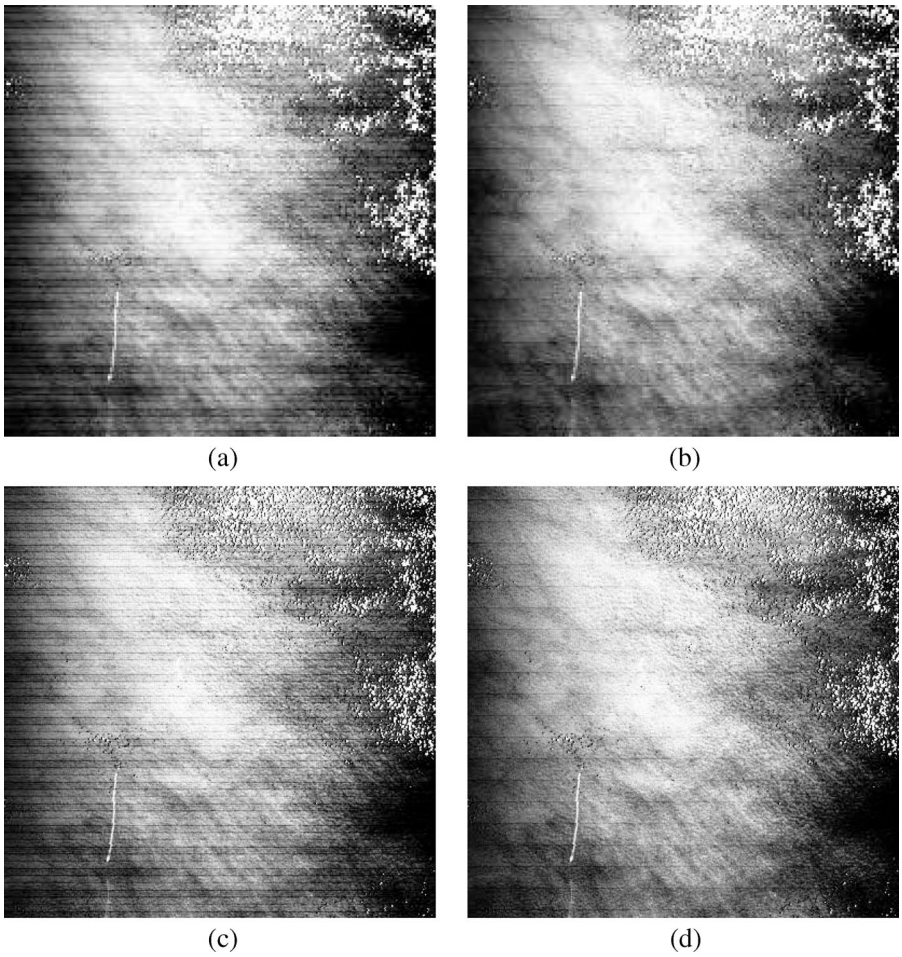

Fig. 10. Subimages of Terra MODIS acquired on June 5, 2005. Image is acquired from Pacific Ocean southeast of Shanghai, China. These images are 200 by 200 pixels (200 by 200 km) for 1000-m resolution subimages and 400 by 400 pixels (200 by 200 km) for 500-m resolution subimages. (a) Terra MODIS band 7 before histogram matching at 1000-m pixel resolution, (b) Terra MODIS band 7 after histogram matching at 1000-m pixel resolution, (c) Terra MODIS band 7 before histogram matching at 500-m pixel resolution, and (d) Terra MODIS band 7 after histogram matching at 500-m pixel resolution.

resolution to test the performance of the local least squares fitting. Figs. 8 and 9 show samples of the Terra MODIS tested image without georectification at 1000- and 500-m pixel resolutions. The images cover a region of the study site over part of Sakhalin Island, Russia. They were acquired on September 5, 2005. The image in Fig. 8 has a size of 200 by 200 pixels (200 by 200 km), whereas the image in Fig. 9 is 400 by 400 pixels (200 by 200 km). The Terra MODIS band 6 images in Figs. 8(c) and 9(c) are corrupted with blank stripes corresponding to the nonfunctional detectors found in Aqua MODIS band 6.

A grayscale transformation is applied for each missing pixel using the relationship between Terra MODIS bands 6 and 7 in order to retrieve the synthetic missing data of Terra MODIS band 6. However, Terra MODIS band 7 reflectance is contaminated by stripe noise that may cause an error in the transformation between bands 6 and 7. Prior to grayscale transformation, a histogram-matching algorithm was applied to correct the stripe noise in Terra MODIS band 7. Fig. 10 shows a typical subsection of Terra MODIS data acquired over the Pacific Ocean southeast of Shanghai, China. Pronounced striping is visible in the original Terra MODIS band 7 data for both 1000- and 500-m-pixel-resolution images [Fig. 10(a) and (c)]. Fig. 10(b) and (d) show the same scenes, but destriped with the use of the histogram matching mentioned in Section III.

Fig. 11 shows the horizontal profile shown in Figs. 8(c) and 9(c). The horizontal profile of the reflectance data is derived from the original Terra MODIS band 6 image, simulated band 6 image, and Terra MODIS band 7 image. The plot shows the sharp transitions between land and ocean surfaces. It can be seen that the amplitude of the MODIS band 7 profile is mostly lower than that of MODIS band 6. This may be why snow at satellite reflectance is typically a few percent lower in NDSI produced by MODIS band 7 than in NDSI produced by MODIS band 6 [15]. Fig. 11 shows that, after restoration by the proposed algorithm, the horizontal profile of the restored image follows the same change trend as in the original image. This indicates that the proposed algorithm introduces little distortion in the spectrum characteristic of Terra MODIS band 6.

The mean difference, standard deviation, and correlation coefficient between simulated and original band 6 reflectance of both 1000- and 500-m grid cells (Tables I and II) are in good agreement in different quarters. The mean difference of each tested scene is less than 10^{-4} for 1000-m and 10^{-2} for 500-m pixel resolutions. Comparing Tables I and II reveals that the mean difference values and standard deviation of 500-m

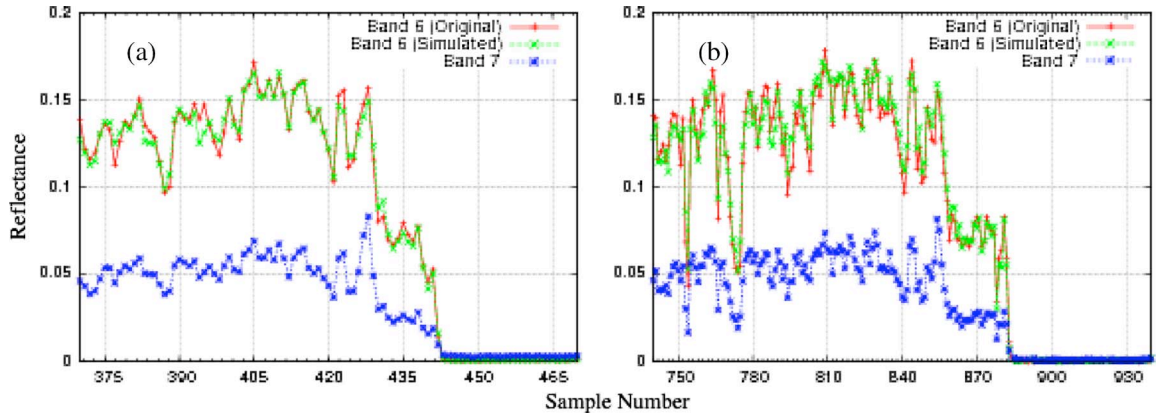

Fig. 11. Horizontal profiles of reflectance of the image data shown in Figs. 8(c) and 9(c) extracted from Terra MODIS. Image was acquired on September 5, 2005 with (a) 1000- and (b) 500-m pixel resolutions.

TABLE I
MEAN DIFFERENCE, STANDARD DEVIATION, AND CORRELATION COEFFICIENT OF THE ORIGINAL TERRA BAND 6 REFLECTANCE AND SIMULATED TERRA BAND 6 REFLECTANCE AT 1000-m PIXEL RESOLUTION

Date	Mean Difference	Standard Deviation	Correlation Coefficient	Regression	RMSE
Feb 9, 2005	-2.50×10^{-5}	0.0039	0.9987	$0.00043 + 0.99549 \times B6$	3.06278×10^{-5}
Jun 5, 2005	6.30×10^{-5}	0.0072	0.9982	$0.00051 + 0.99719 \times B6$	3.60309×10^{-5}
Sep 5, 2005	-6.30×10^{-5}	0.0123	0.9945	$0.00025 + 0.99842 \times B6$	2.79670×10^{-5}
Dec 2, 2005	9.19×10^{-4}	0.0032	0.9988	$0.00059 + 1.00368 \times B6$	2.95640×10^{-5}

TABLE II
SAME AS TABLE I, EXCEPT FOR 500-m PIXEL RESOLUTION

Date	Mean Difference	Standard Deviation	Correlation Coefficient	Regression	RMSE
Feb 9, 2005	4.90×10^{-5}	0.0062	0.9969	$0.00052 + 0.99535 \times B6$	2.24889×10^{-5}
Jun 5, 2005	-6.40×10^{-5}	0.0158	0.9918	$0.00084 + 0.99528 \times B6$	2.24072×10^{-5}
Sep 5, 2005	-1.11×10^{-2}	0.1105	0.7580	$0.00030 + 0.99649 \times B6$	1.97033×10^{-5}
Dec 2, 2005	-1.32×10^{-3}	0.0222	0.9497	$0.00013 + 0.98871 \times B6$	2.22283×10^{-5}

grid cells are higher than those of 1000-m grid cells, whereas the correlation coefficient of 500-m grid cells is lower than that of 1000-m grid cells. This is because there are more missing data in 500-m grid cells than in 1000-m grid cells.

Figs. 12 and 13 show the scatter plots between the original Terra MODIS band 6 and the Terra MODIS band 7 simulated band 6 reflectance in 1000- and 500-m resolutions. The specific regression relationships are listed in Tables I and II. Ideally, the slope of the regression function should be near unity and y-intercept near zero. In Figs. 12 and 13, the scatter around the regression line in each of the scenes tested appears about the same with a little more scatter in Fig. 13. This trend is borne out in Table II, indicating that the root-mean-square errors (rmse) are a little lower in Fig. 6(c) than in the others. It should be noted that the correlation coefficient of Fig. 6(c) is lower than the others because Terra MODIS band 7 is contaminated by noise when the signal is low. In the other words, the ocean region of Terra MODIS band 7 is contaminated by random noise. It should also be noted that, in terms of correlation coefficient and rmse, they are very similar.

B. Performance Evaluation of Detector-to-Detector Stripe Elimination

Figs. 14 and 15 show samples of the Aqua MODIS tested images without georectification at 1000- (Fig. 14) and 500-m (Fig. 15) pixel resolutions. The images cover a part of Laihou Wan, China, and are upside down due to the ascending mode of Aqua spacecraft's flight. They were acquired on June 11, 2005. Fig. 14(b) shows an original image of Aqua MODIS band 6 at 1000-m pixel resolution. The image is badly contaminated by stripe noise of nonfunctional detectors. Fig. 15(b) shows the smooth texture of the original Aqua MODIS band 6 image at 500-m pixel resolution. The smoothness of this image is due to interpolation of the missing data. Figs. 14(c) and 15(c) show the improvement of data quality after applying the proposed algorithm. Fig. 16 shows the range data of the vertical profile shown in Figs. 14(c) and 15(c). The original range image consists of land and sea surfaces. Fig. 16(a) shows the abrupt change in the original band 6 profile of the 1000-m grid cell due to the reflectance of the missing data being equal to -1. Fig. 16(b) shows the gradual change over the

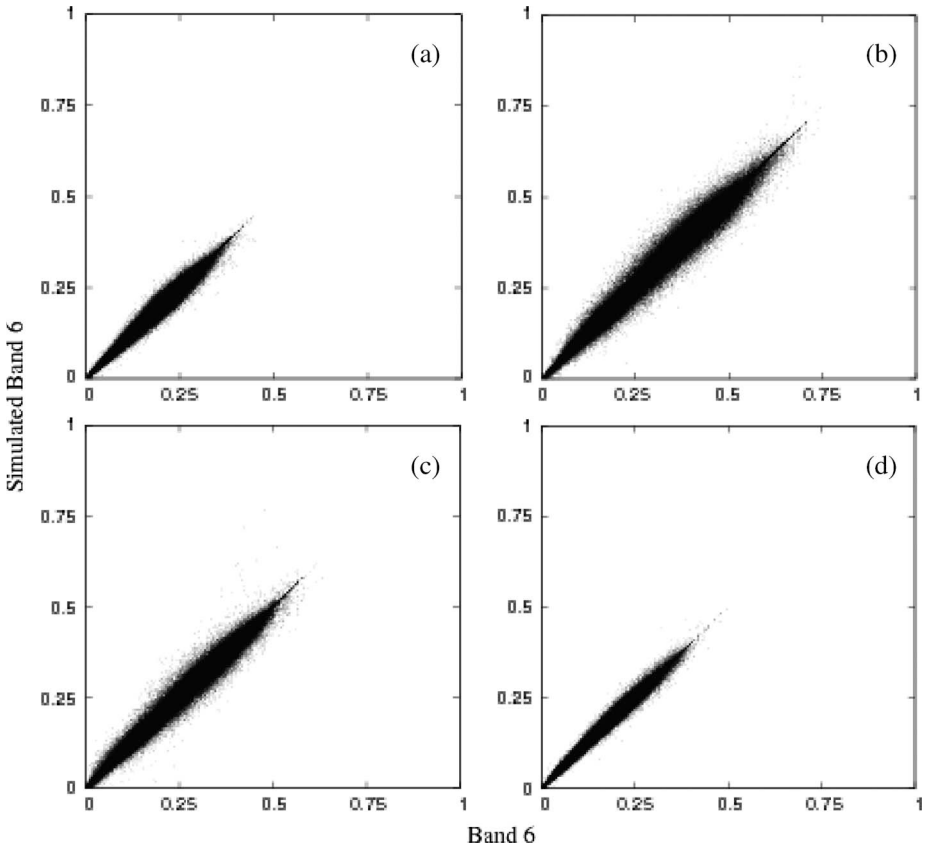

Fig. 12. Scatter plots of reflectance of Terra MODIS band 6 to its simulated band 6 in 1000-m pixel resolution. Terra MODIS images were acquired on (a) February 9, 2005, (b) June 5, 2005, (c) September 5, 2005, and (d) December 2, 2005.

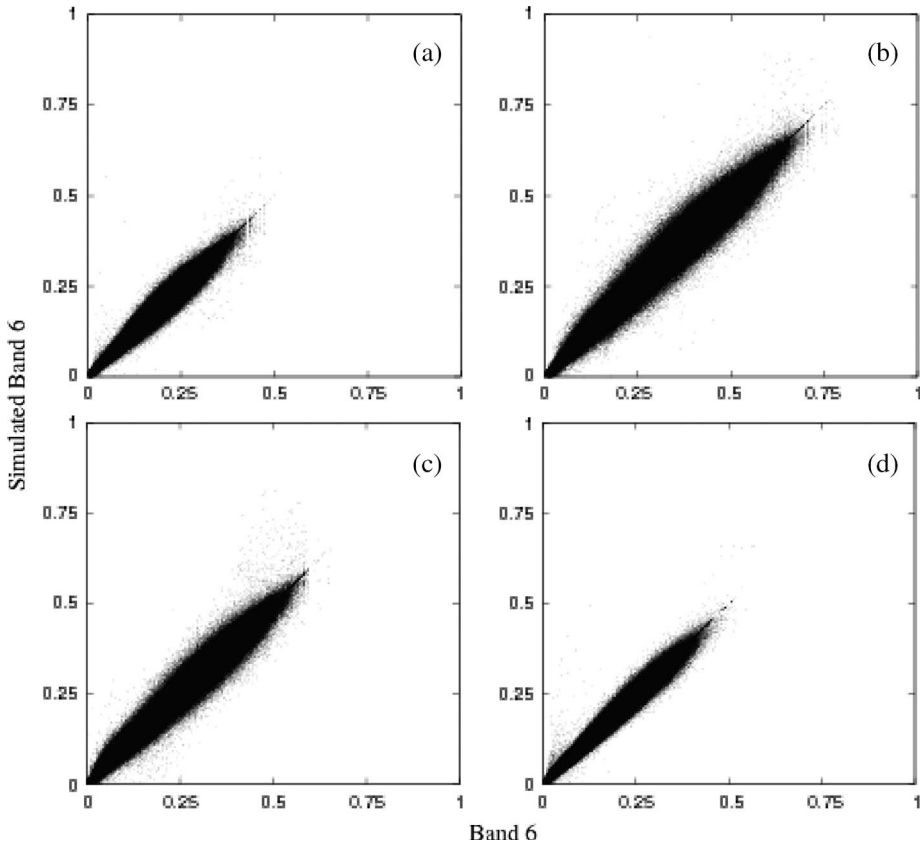

Fig. 13. Same as Fig. 12 except Terra MODIS band 6, and its simulated one has 500-m pixel resolution.

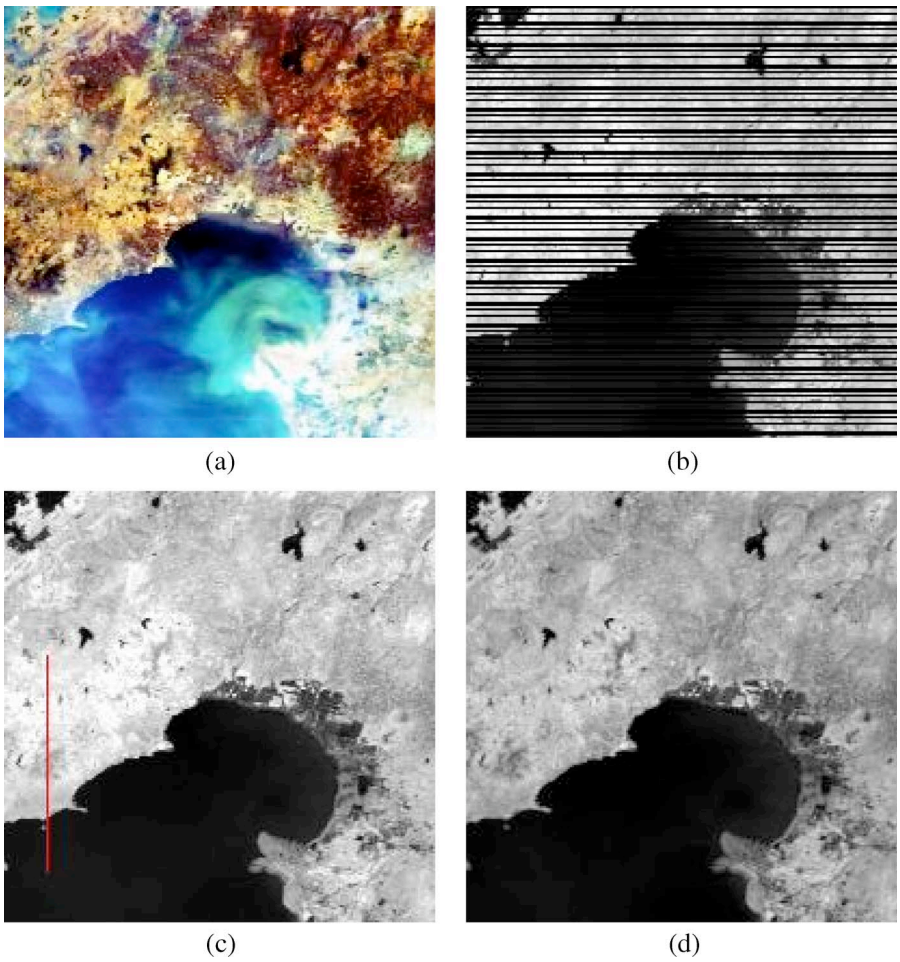

Fig. 14. Subimages of Aqua MODIS of 1000-m pixel resolution acquired on June 11, 2005. Upside-down image was acquired over Laihou Wan, China. This image is 200 by 200 pixels (200 by 200 km). (a) True color composite $R =$ band1, $G =$ band4, $B =$ band3, (b) original Aqua MODIS band 6, and (c) restored Aqua MODIS bands 6 and (d) 7.

original profile of the 500-m grid cell due to the missing data being interpolated from the nearest functional detectors. Fig. 16 shows that the proposed algorithm can recover most of the missing data.

Fig. 17 shows the Fourier transforms of the Aqua MODIS band 6's test images before and after restoration, with and without applying histogram matching. The spectrum depicted in these images is the ensemble-averaged power spectrum computed across the rows of the scene and plotted as a function of normalized frequency. For better visualization of noise reduction by the proposed method, very high spectral magnitudes are not plotted. This provides a better range for the frequency components of the spectrum, where the noise is located. The inputs of the fast Fourier transform were 2030 row vectors.

Fig. 17 clearly shows that the pulses in the frequency domain, which are contaminated by the detector-to-detector striping, are significantly reduced by the histogram matching. For 1000-m-pixel-resolution data, the detector-to-detector stripe noise in Aqua MODIS images is narrowband at frequencies of 1/10, 2/10, 3/10, 4/10, and 5/10 cycles per pixel. For 500-m-pixel-resolution data, stripe noise pulses are located at frequencies of 1/20, 2/20, 3/20, 4/20, 5/20, 6/20, 7/20, 8/20, 9/20, and 10/20 cycles per pixel.

For quantitative measurement, the ratio of noise reduction (NR) was employed as a quality index. The NR has been used in [18]–[20] which is calculated from

$$\mathrm{NR} = \frac{N_o}{N_k} \tag{6}$$

where N_o stands for the power of the frequency components produced by stripe noise in the original image and N_k stands for the power of the frequency components produced by stripe noise in the destriped images. Stripe noise components of the spectrum can be calculated by

$$N_i = \sum_{\mathrm{BW}_N} P_i(D) \tag{7}$$

where $P_i(D)$ is the averaged power spectrum down the columns of an image (where D is the distance from the origin in Fourier space); BW_N is the stripe noise region of the spectrum; $D \in \{0.1, 0.2, 0.3, 0.4, 0.5\}$ for detector-to-detector striping of 1000-m pixel resolution with addition of $D \in \{0.05, 0.15, 0.25, 0.35, 0.45\}$ if they are images with 500-m pixel resolution.

Each step of the algorithm, including the original image, the restoration output without histogram matching, and the

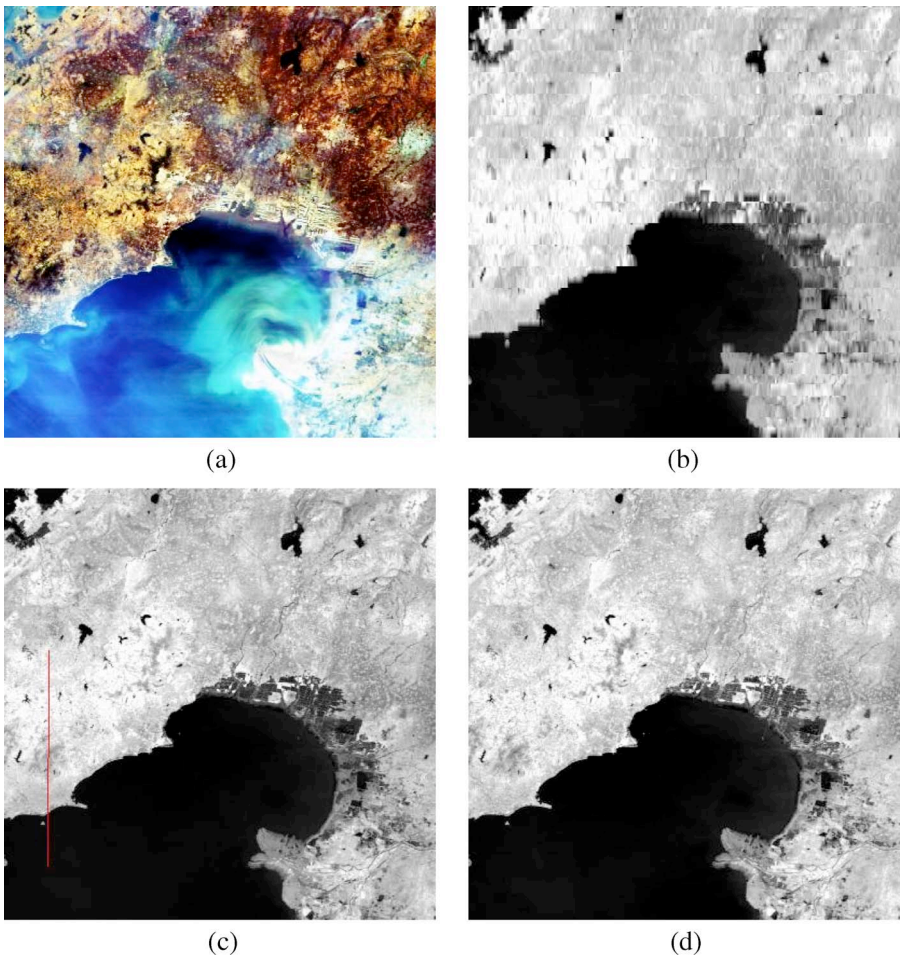

Fig. 15. Same as Fig. 14 except for 500-m pixel resolution, and this image is 400 by 400 pixels (200 by 200 km).

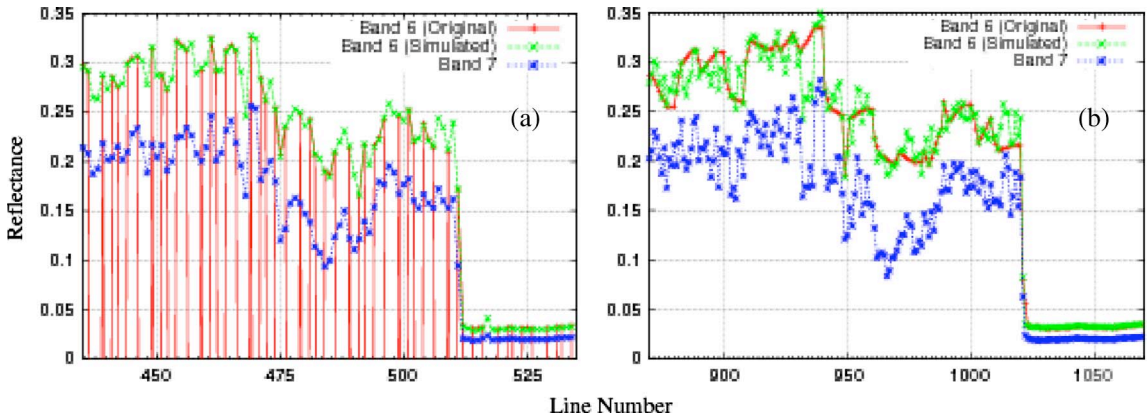

Fig. 16. Vertical profiles of reflectance of the image data shown in Figs. 14(c) and 15(c) extracted from Aqua MODIS. Image was acquired on June 11, 2005 with (a) 1000- and b) 500-m pixel resolutions.

restoration output with histogram matching, is separately analyzed in order to investigate the effectiveness of the reduction of stripe noise reduction. The NR results are reported in Tables III and IV. The mean values of NR are 3.907×10^7, 1.0264×10^6, 28.151, and 1.129 for the restoration with and without histogram matching at 1000- and 500-m pixel resolutions. These show that the restoration with histogram matching increases the NR by a factor of 38 for 1000-m and 25 for 500-m pixel resolutions.

V. Conclusion

This paper has presented a method to restore Aqua MODIS band 6 using histogram matching combined with local least squares fitting. This is because 15 of the 20 detectors in Aqua MODIS band 6 are either nonfunctional or noisy. Histogram matching is used for removing detector-to-detector striping of the functional detectors. Local least squares fitting is used for restoring the missing data of the nonfunctional detectors. The Aqua MODIS image data used in this research are in DN

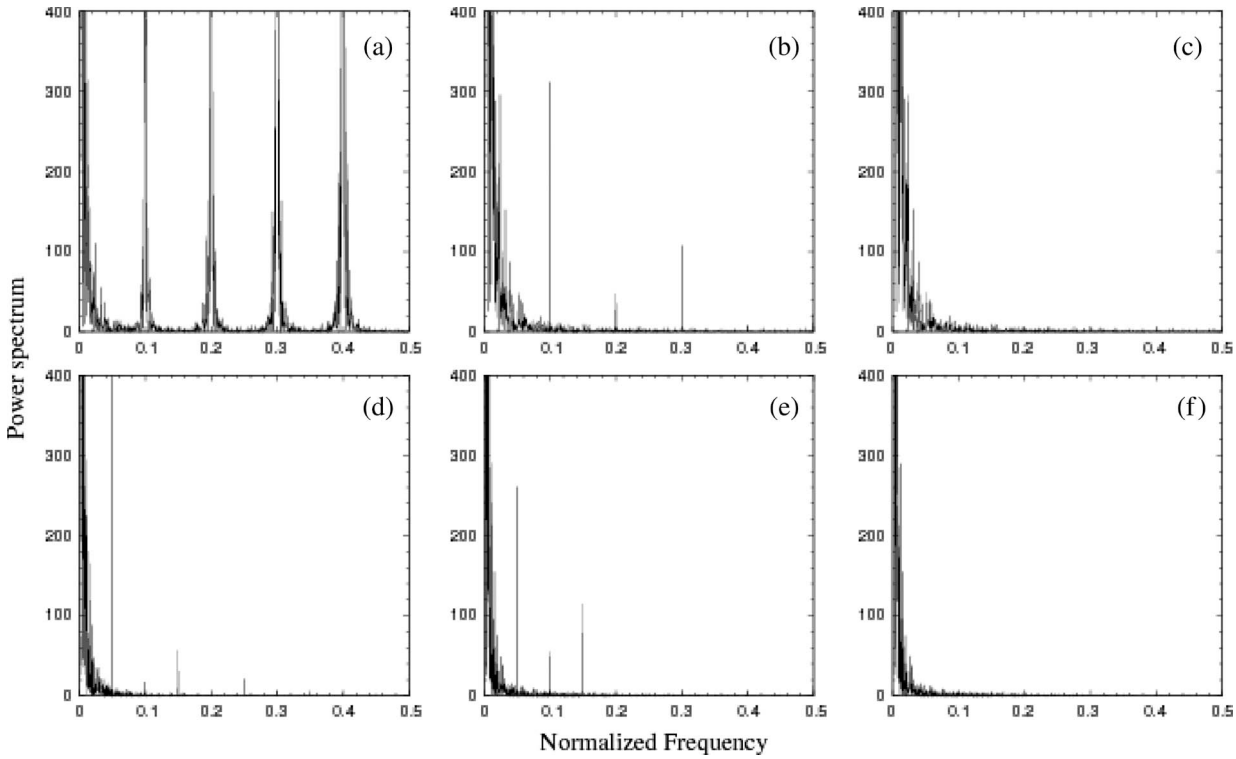

Fig. 17. Mean column power spectrum of Aqua MODIS band 6 images acquired on November 6, 2005. (a) Original 1000-m pixel resolution image, (b) after restoring of 1000-m pixel resolution image (without histogram matching), (c) after restoring of 1000-m pixel resolution image (with histogram matching), (d) original 500-m pixel resolution image, (e) after restoring of 1000-m pixel resolution image (without histogram matching), and (f) after restoring of 1000-m pixel resolution image (with histogram matching).

TABLE III
NOISE REDUCTION RATIO OF THE ORIGINAL AQUA MODIS BAND 6 AT 1000-m PIXEL RESOLUTION, ITS RESTORATION OUTPUT WITHOUT HISTOGRAM MATCHING, AND ITS RESTORATION OUTPUT WITH HISTOGRAM-MATCHING

Date	Original	Without histogram	With histogram
Feb 2, 2005	1	1.040×10^6	6.073×10^7
Jun 11, 2005	1	8.324×10^5	2.098×10^7
Sep 7, 2005	1	1.349×10^6	4.219×10^7
Dec 2, 2005	1	8.842×10^5	3.239×10^7

TABLE IV
SAME AS TABLE III, EXCEPT FOR 500-m PIXEL RESOLUTION

Date	Original	Without histogram	With histogram
Feb 2, 2005	1	0.967	30.776
Jun 11, 2005	1	1.162	24.843
Sep 7, 2005	1	1.243	28.724
Dec 2, 2005	1	1.144	28.262

format and are not georectified. The proposed method can be applied for both 1000- and 500-m pixel resolutions. The results demonstrate that the proposed algorithm can restore the missing data with little distortion. Local least squares fitting was validated by employing such measures as correlation coefficient and rmse. Over all the scenes used in this paper, the correlation coefficients were around 0.99 and rmse were around 2×10^{-5}. The stripe noise reduction ratio was calculated to validate the effectiveness of the histogram matching. Compared with the previous algorithm [14], the proposed algorithm can be applied effectively to Aqua MODIS band 6 images without regard to land cover types, spectral characteristics, or scan geometry. Its computation time is also satisfactory for operational use. Some MODIS products and applications could benefit from this proposed method such as the aerosol product (MOD04), snow cover product (MOD06), and cloud-mask product (MOD35).

ACKNOWLEDGMENT

The authors would like to thank the Ministry of Education, Culture, Sports, Science and Technology, Japan Government for the Ph.D. scholarship at The University of Tokyo.

REFERENCES

[1] W. L. Barnes, T. S. Pagano, and V. V. Salomonson, "Prelaunch characteristics of the Moderate Resolution Imaging Spectroradiometer (MODIS) on EOS-AM1," *IEEE Trans. Geosci. Remote Sens.*, vol. 36, no. 4, pp. 1088–1100, Jul. 1998.

[2] B. Guenther, G. D. Godden, X. Xiong, E. J. Knight, S. Y. Qiu, H. Montgomery, M. M. Hopkins, M. G. Khayat, and Z. Hao, "Prelaunch algorithm and data format for the level 1 calibration products for the EOS-AM1 Moderate Resolution Imaging Spectroradiometer (MODIS)," *IEEE Trans. Geosci. Remote Sens.*, vol. 36, no. 4, pp. 1142–1151, Jul. 1998.

[3] C. O. Justice, E. Vermote, J. R. G. Townshend, R. Defries, D. P. Roy, D. K. Hall, V. V. Salomonson, J. L. Privette, G. Riggs, A. Strahler, W. Lucht, R. B. Myneni, Y. Knyazikhin, S. W. Running, R. R. Nemani, Z. M. Wan, A. R. Huete, W. van Leeuwen, R. E. Wolfe, L. Giglio, J. P. Muller, P. Lewis, and M. J. Barnsley, "The Moderate Resolution Imaging Spectroradiometer (MODIS): Land remote sensing for global

change research," *IEEE Trans. Geosci. Remote Sens.*, vol. 36, no. 4, pp. 1228–1249, Jul. 1998.
[4] B. Guenther, X. Xiong, V. V. Salomonson, W. L. Barnes, and J. Young, "On-orbit performance of the Earth observing system moderate resolution imaging spectroradiometer; first year of data," *Remote Sens. Environ.*, vol. 83, no. 1, pp. 16–30, Nov. 2002.
[5] Z. Wan, "Estimate of noise and systematic error in early thermal infrared data of the Moderate Resolution Imaging Spectroradiometer (MODIS)," *Remote Sens. Environ.*, vol. 80, no. 1, pp. 47–54, Apr. 2002.
[6] W. L. Barnes, X. Xiong, and V. V. Salomonson, "Status of terra MODIS and aqua MODIS," *Adv. Space Res.*, vol. 32, no. 11, pp. 2099–2106, Dec. 2003.
[7] X. Xiong, W. L. Barnes, B. Guenther, and R. E. Murphy, "Lessons learned from MODIS," *Adv. Space Res.*, vol. 32, no. 11, pp. 2107–2112, Dec. 2003.
[8] X. Xiong, K. Chiang, J. Esposito, B. Guenther, and W. Barnes, "MODIS on-orbit calibration and characterization," *Metrologia*, vol. 40, no. 1, pp. S89–S92, Feb. 2003.
[9] X. Xiong, N. Z. Che, and W. Barnes, "Terra MODIS on-orbit spatial characterization and performance," *IEEE Trans. Geosci. Remote Sens.*, vol. 43, no. 2, pp. 355–365, Feb. 2005.
[10] X. Xiong, N. Z. Che, and W. L. Barnes, "Terra MODIS on-orbit spectral characterization and performance," *IEEE Trans. Geosci. Remote Sens.*, vol. 44, no. 8, pp. 2198–2206, Aug. 2006.
[11] X. Xiong, J. Q. Sun, W. Barnes, V. Salomonson, J. Esposito, H. Erives, and B. Guenther, "Multiyear on-orbit calibration and performance of terra MODIS reflective solar bands," *IEEE Trans. Geosci. Remote Sens.*, vol. 45, no. 4, pp. 879–889, Apr. 2007.
[12] MODIS Characterization Support Team, *MODIS level 1B products data dictionary*, 2005. MCST Internal Memorandum # M1055. [Online]. Available: http://www.mcst.ssai.biz/mcstweb/L1B/product.html
[13] V. V. Salomonson and I. Appel, "Development of the aqua MODIS NDSI fractional snow cover algorithm and validation results," *IEEE Trans. Geosci. Remote Sens.*, vol. 44, no. 7, pp. 1747–1756, Jul. 2006.
[14] L. L. Wang, J. J. Qu, X. Siong, H. Xianjun, X. Yong, and C. Nianzeng, "A new method for retrieving band 6 of Aqua MODIS," *IEEE Geosci. Remote Sens. Lett.*, vol. 3, no. 2, pp. 267–270, Apr. 2006.
[15] L. L. Wang, J. J. Qu, H. Jack Xiong, X. Xianjun, and C. Yong, "A preliminary study of aqua/MODIS snow coverage continuity with simulated band 6," in *Proc. SPIE Annu. Conf.*, San Diego, CA, Aug. 13–17, 2006.
[16] L. Gumley, *URL: Western Australian satellite technology and applications consortium*, Nov. 26–29, 2002. [Online]. Available: http://www.wastac.wa.gov.au/modis_workshop_2002/Lecture_3_Scanner_Characteristics_Image_Artifacts_Destriping.ppt
[17] J. J. Pan and C. I. Chang, "Destriping of Landsat MSS images by filtering techniques," *Photogramm. Eng. Remote Sens.*, vol. 58, no. 10, pp. 1417–1423, 1992.
[18] J. J. Simpson, J. I. Gobat, and R. Frouin, "Improved destriping of GOES images using finite impulse response filters," *Remote Sens. Environ.*, vol. 52, no. 1, pp. 15–35, Apr. 1995.
[19] J. S. Chen, Y. Shao, H. D. Guo, W. Wang, and B. Zhu, "Destriping CMODIS data by power filtering," 2*IEEE Trans. Geosci. Remote Sens.*, vol. 41, no. 9, pp. 2119–2124, Sep. 2003.
[20] P. Rakwatin, W. Takeuchi, and Y. Yasuoka, "Stripe noise reduction in MODIS data by combining histogram matching with facet filter," *IEEE Trans. Geosci. Remote Sens.*, vol. 45, no. 6, pp. 1844–1856, Jun. 2007.
[21] B. K. P. Horn and R. J. Woodham, "Destriping Landsat MSS images by histogram modification," *Comput. Graph. Image Process.*, vol. 10, pp. 69–83, 1979.
[22] D. J. Poros and C. J. Peterson, "Methods for destriping Landsat Thematic Mapper images—A feasibility study for an online destriping Landsat Thematic Mapper Image Processing System (TIPS)," *Photogramm. Eng. Remote Sens.*, vol. 51, pp. 1371–1378, 1985.
[23] M. P. Weinreb, R. Xie, J. H. Lienesch, and D. S. Crosby, "Destriping GOES images by matching empirical distribution functions," *Remote Sens. Environ.*, vol. 29, no. 2, pp. 185–195, Aug. 1989.
[24] M. Wegener, "Destriping multiple detector imagery by improved histogram matching," *Int. J. Remote Sens.*, vol. 11, no. 5, pp. 859–875, 1990.
[25] D. L. Helder, B. Quirk, and J. Hood, "A technique for the reduction of banding in Landsat TM images," *Photogramm. Eng. Remote Sens.*, vol. 58, pp. 1425–1431, 1992.
[26] D. L. Helder and B. K. Quirk, "Landsat thematic mapper reflective-band radiometric artifacts," *IEEE Trans. Geosci. Remote Sens.*, vol. 42, no. 12, pp. 2704–2716, Dec. 2004.
[27] D. Tanre, Y. J. Kaufman, M. Herman, and S. Mattoo, "Remote sensing of aerosol properties over oceans using the MODIS/EOS spectral radiances," *J. Geophys. Res.*, vol. 102, no. D14, pp. 16 971–16 988, 1997.
[28] A. Ignatov, P. Minnis, N. Loeb, B. A. Wielicki, W. F. Miller, S. Sun-Mack, D. Tanre, L. Remer, I. Laszlo, and E. Geier, "Two MODIS aerosol products over ocean on the terra and aqua CERES SSF datasets," *J. Atmos. Sci.*, vol. 62, no. 4, pp. 1008–1031, Apr. 2005.
[29] A. Ignatov, P. Minnis, W. F. Miller, B. A. Wielicki, and L. Remer, "Consistency of global MODIS aerosol optical depths over ocean on terra and aqua CERES SSF data sets," *J. Geophys. Res.*, vol. 111, p. D14 202, 2006. DOI: 10.1029/2005JD006645.
[30] V. V. Salomonson and I. Appel, "Estimating fractional snow cover from MODIS using the normalized difference snow index," *Remote Sens. Environ.*, vol. 89, no. 3, pp. 351–360, Feb. 2004.
[31] D. K. Hall, G. A. Riggs, and V. V. Salomonson, "Development of methods for mapping global snow cover using moderate resolution imaging spectroradiometer data," *Remote Sens. Environ.*, vol. 34, no. 2, pp. 127–140, Nov. 1995.
[32] D. K. Hall, G. A. Riggs, V. V. Salomonson, N. E. DeGirolamo, and K. J. Bayr, "MODIS snow-cover products," *Remote Sens. Environ.*, vol. 83, no. 1, pp. 181–194, Nov. 2002.
[33] S. Platnick, M. D. King, S. A. Ackerman, W. P. Menzel, B. A. Baum, J. C. Riedi, and R. A. Frey, "The MODIS cloud products: Algorithms and examples from Terra," *IEEE Trans. Geosci. Remote Sens.*, vol. 41, no. 2, pp. 459–473, Feb. 2003.
[34] S. Ackerman, K. Strabala, P. Menzel, R. Frey, C. Moeller, and L. Gumley, "Discriminating clear sky from clouds with MODIS," *J. Geophys. Res.*, vol. 103, no. D24, pp. 32 141–32 157, 1998.
[35] P. Pilewskie and S. Twomey, "Cloud phase discrimination by reflectance measurements near 1.6 and 2.2 μm," *J. Atmos. Sci.*, vol. 44, no. 22, pp. 3419–3420, 1987.
[36] B. A. Baum and J. D. Spinhirne, "Remote sensing of cloud properties using MODIS airborne simulator imagery during SUCCESS 3. Cloud overlap," *J. Geophys. Res.*, vol. 105f, no. D9, pp. 11 793–11 804, 2000.
[37] S. L. Nasiri and B. A. Baum, "Daytime multilayered cloud detection using multispectral imagery data," *J. Atmos. Ocean. Technol.*, vol. 21, no. 8, pp. 1145–1155, 2004.
[38] M. J. Pavolonis and A. K. Heidinger, "Daytime cloud overlap detection from AVHRR and VIIRS," *J. Appl. Meteorol.*, vol. 43, no. 5, pp. 762–778, 2004.
[39] M. J. Pavolonis, A. K. Heidinger, and T. Uttal, "Daytime global cloud typing from AVHRR and VIIRS: Algorithm description, validation, and comparisons," *J. Appl. Meteorol.*, vol. 44, no. 6, pp. 804–826, 2005.
[40] R. Fensholt and I. Sandholt, "Derivation of a shortwave infrared water stress index from MODIS near- and shortwave infrared data in a semiarid environment," *Remote Sens. Environ.*, vol. 87, no. 1, pp. 111–121, Sep. 2003.
[41] A. Baccini, M. A. Friedl, C. E. Woodcock, R. Warbington, and L. Remer, "Forest biomass estimation over regional scales using multisource data," *J. Geophys. Res. Lett.*, vol. 31, no. 10, p. L10 501, 2004.
[42] F. M. Gemmell, "Effects of forest cover, terrain, and scale on timber volume estimation with thematic mapper data in a Rocky mountain site," *Remote Sens. Environ.*, vol. 51, no. 2, pp. 291–305, Feb. 1995.
[43] W. B. Cohen and T. A. Spies, "Estimating structural attributes of Douglas-fir/western hemlock forest stands from Landsat and SPOT imagery," *Remote Sens. Environ.*, vol. 41, no. 1, pp. 1–17, Jul. 1992.
[44] C. B. Puhr and D. N. M. Donoghue, "Remote sensing of upland conifer plantations using Landsat TM data: A case study from Galloway, south-west Scotland," *Int. J. Remote Sens.*, vol. 21, no. 4, pp. 633–646, Mar. 2002.

Preesan Rakwatin received the B.Eng. degree in electrical engineering from the Kasetsart University, Bangkok, Thailand, in 1998, the M.Eng. degree from the Asian Institute of Technology, Pathumthani, Thailand, in 2004, and the Ph.D. degree in civil engineering from the University of Tokyo, Tokyo, Japan, in 2007.

Since October 2007, he has been with the Earth Observation Research Center, Space Applications Mission Directorate, Japan Aerospace Exploration Agency, Tsukuba, Japan, as a Visiting Researcher. His research interests include image processing and remote sensing.

Wataru Takeuchi received the B.Eng., M.Eng., and Ph.D. degrees in civil engineering from The University of Tokyo, Tokyo, Japan, in 1999, 2001, and 2004, respectively.

He is currently an Assistant Professor with the Institute of Industrial Science, The University of Tokyo. His research interests include agriculture remote sensing and image processing.

Yoshifumi Yasuoka (M'88–SM'89) received the B.Eng., M.Eng. and Ph.D. degrees in applied physics and mathematics from The University of Tokyo, Tokyo, Japan, in 1970, 1972, and 1975, respectively.

He was with the National Institute for Environmental Studies (NIES), Tsukuba, Japan, from 1975 to 1998, serving as a Researcher, Senior Researcher, and Section Head of the Environmental Information Division. During his two years at NIES, he was the Director of the Center for Global Environmental Research. From 1998 to 2007, he was a Professor with the Institute of Industrial Science, The University of Tokyo, Tokyo, Japan. He is currently a Executive Director of the National Institute for Environmental Studies (NIES), Tsukuba, Japan. His major research field is remote sensing, geographic information system, and spatial data analysis for environment and disaster assessment.

Dr. Yasuoka was the President of the Japan Remote Sensing Society from 2002 to 2004.